Supplementary Material for:

A convenient method of ternary alloys design for CO_2-to-C_2H_4 electroreduction

Yiyang Xiao[a,b], Yingju Yang[a,b,c,*], Wei Liu[a,b], Jing Liu[a,b,c]

[a] State Key Laboratory of Coal Combustion, Huazhong University of Science and Technology, Wuhan 430074, China

[b] School of Energy and Power Engineering, Huazhong University of Science and Technology, Wuhan 430074, China

[c] Shenzhen Institute of Huazhong University of Science and Technology, Shenzhen 518000, China

*Corresponding to: yangyingju@hust.edu.cn

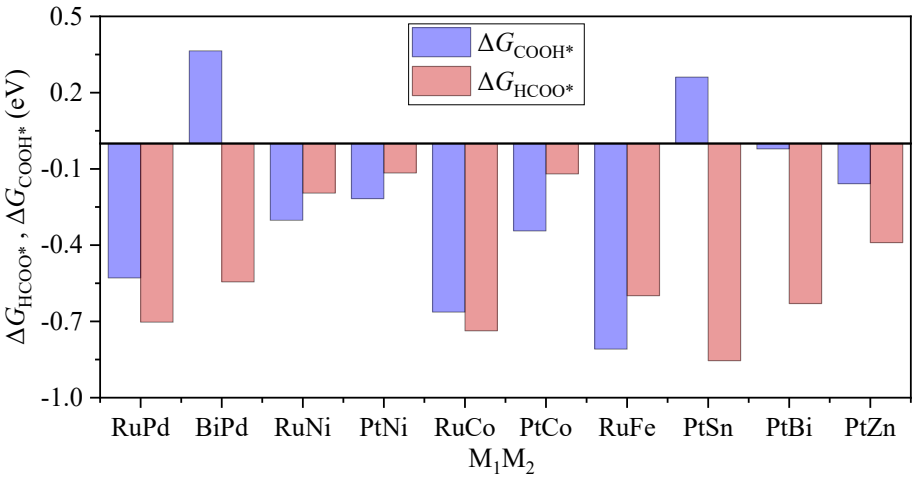

Fig. S1. Comparison of ΔG_{COOH*} and ΔG_{HCOO*} of M_1M_2@Cu catalysts with high CO_2RR selectivity.

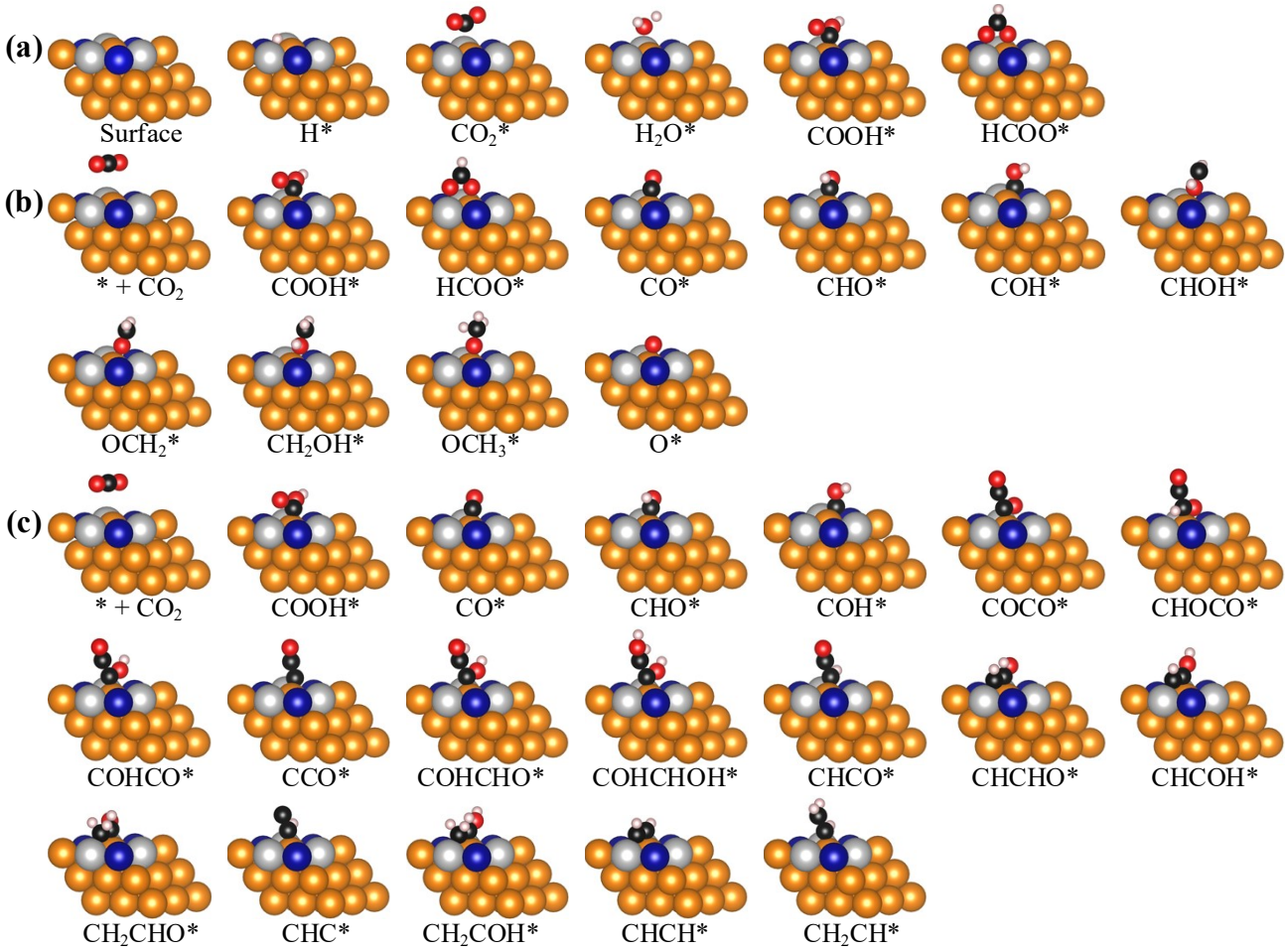

Fig. S2. Optimized structures of intermediates of catalysts screening and CO_2 reduction over M_1M_2@Cu surface. (a) Optimized structures of catalysts screening. (b) Intermediates of CO_2 electrochemical reduction to C_1 products over catalyst surface. (c) Intermediates of CO_2 electrochemical reduction to C_2H_4 over catalyst surface.

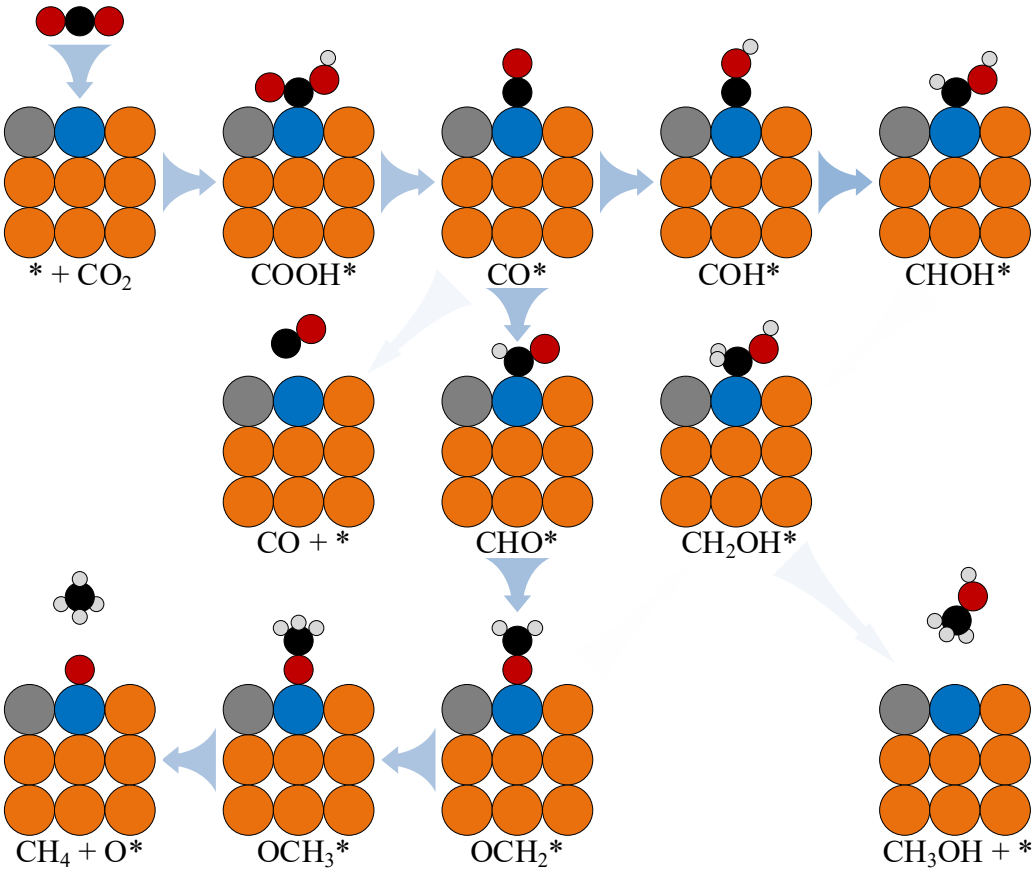

Fig. S3. Reaction network of C_1 products CO, CH_3OH and CH_4.

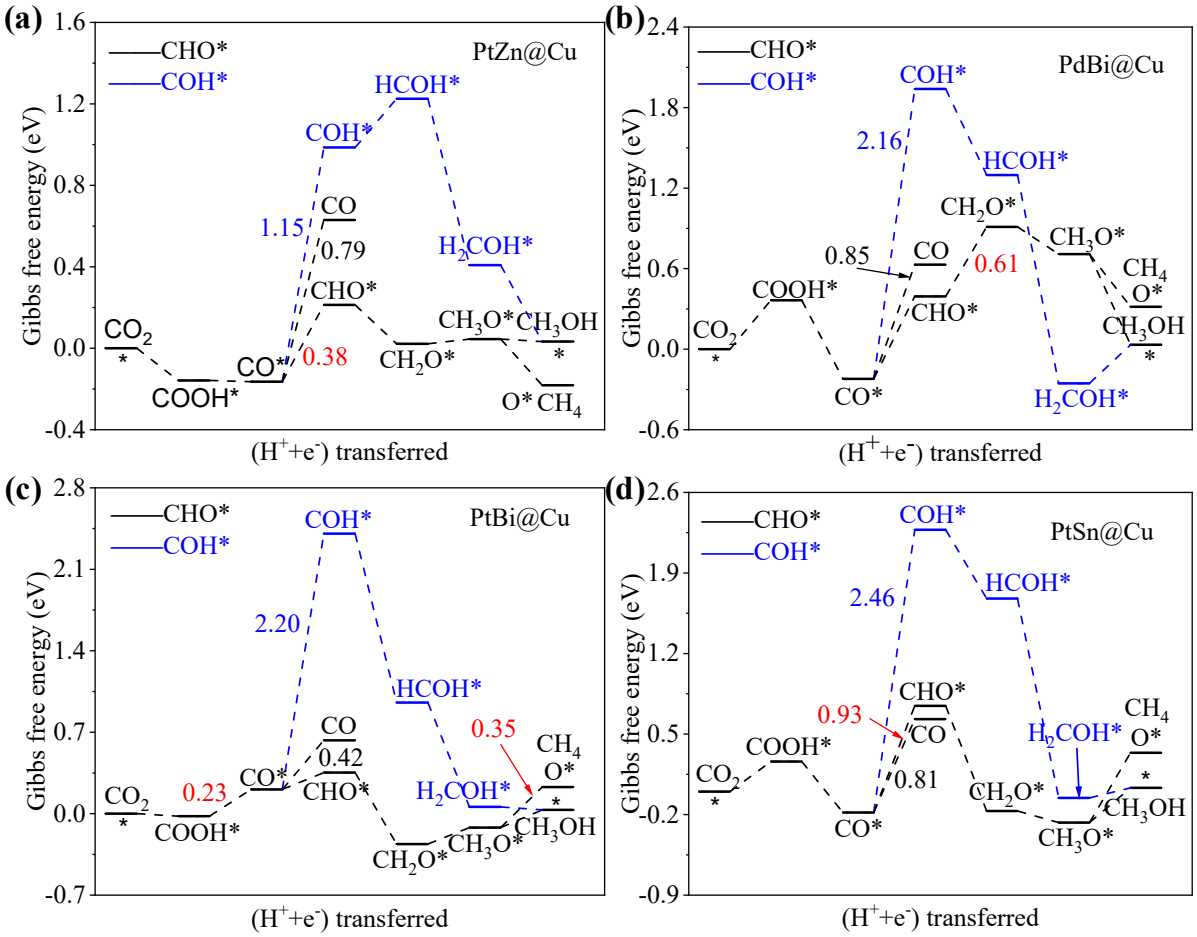

Fig. S4. Gibbs free energy diagram of C_1 products formation. (a) PtZn@Cu. (b) PdBi@Cu. (c) PtBi@Cu. (d) PtSn@Cu.

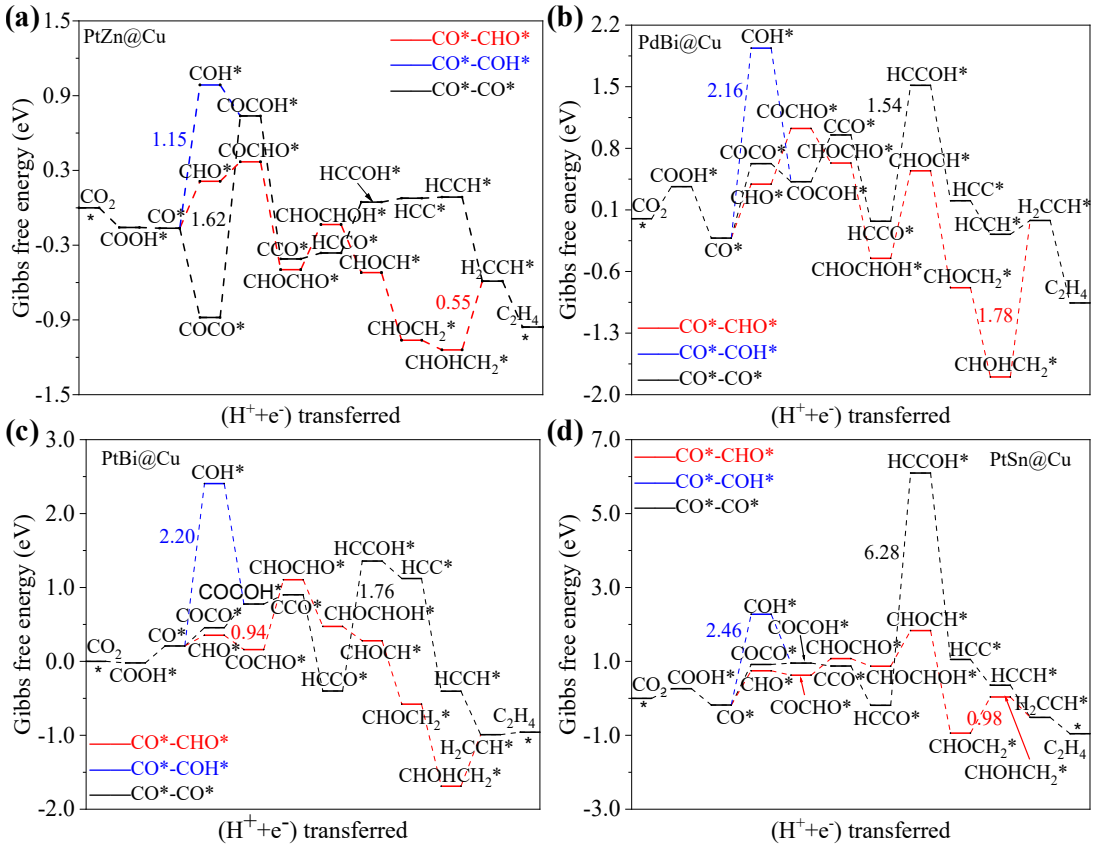

Fig. S5. Gibbs free energy diagram of C_2H_4 formation. (a) PtZn@Cu. (b) PdBi@Cu. (c) PtBi@Cu. (d) PtSn@Cu.

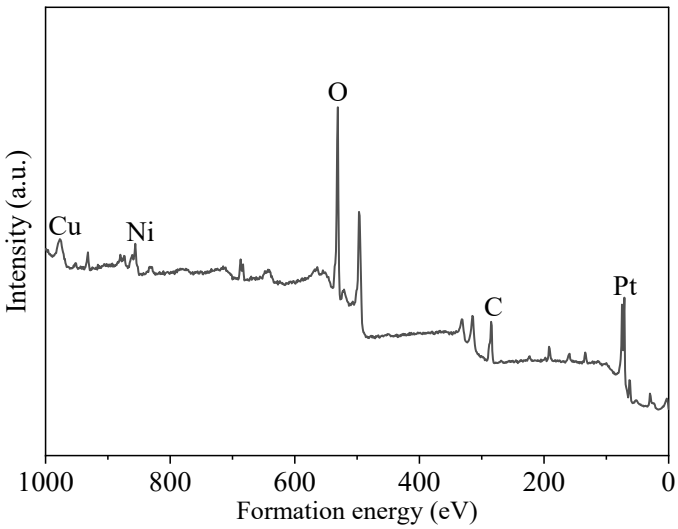

Fig. S6. XPS spectra of PtNi@Cu catalyst.

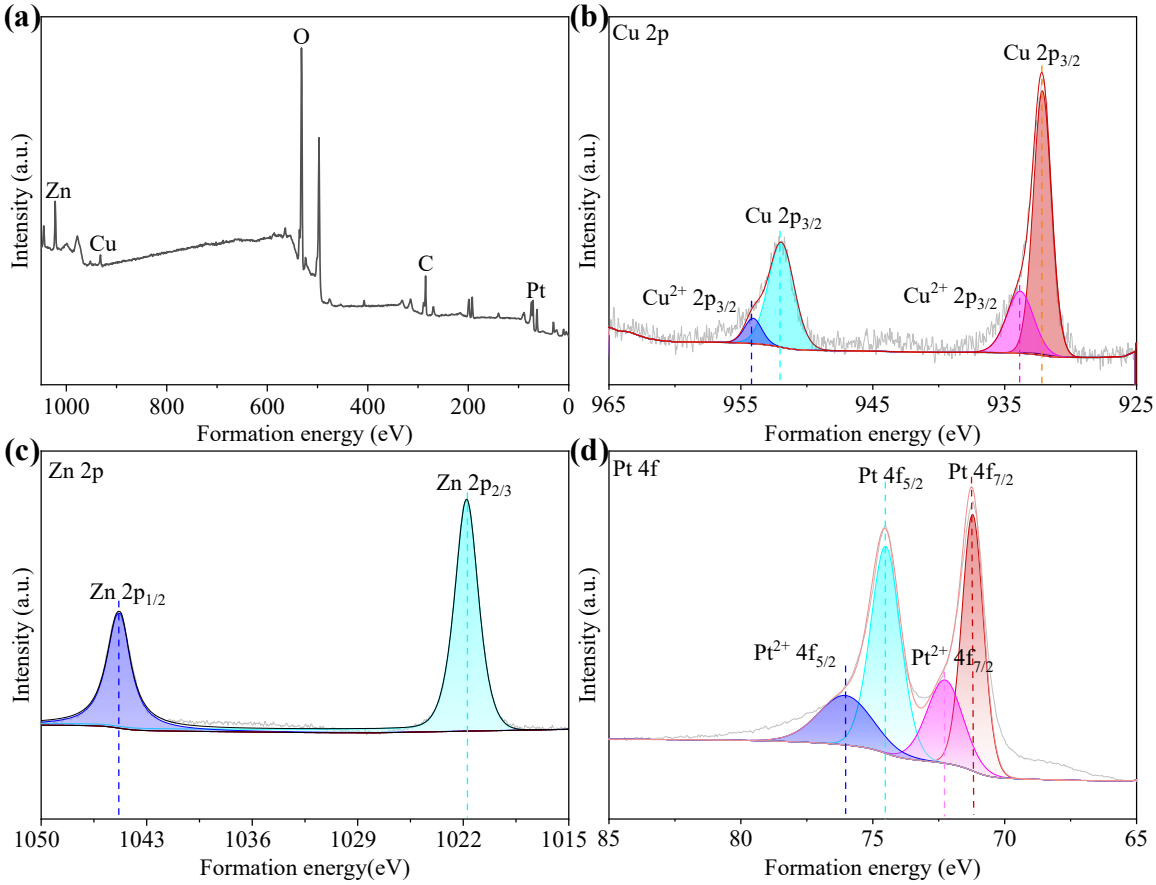

Fig. S7. XPS results of PtZn@Cu catalyst. (a) Survey spectra. (b) Cu 2p XPS spectra. (c) Zn 2p XPS spectra. (d) Pt 2p XPS spectra.

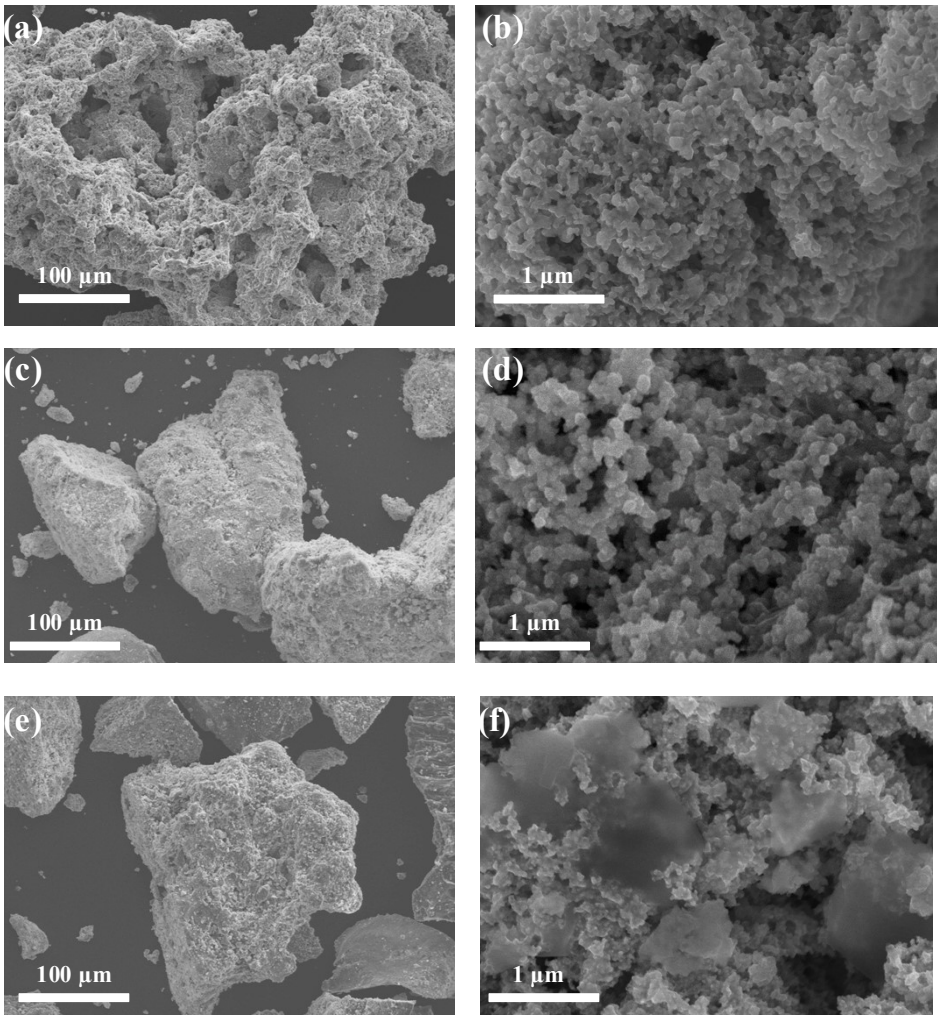

Fig. S8. SEM images of Cu, PtNi@Cu and PtZn@Cu. (a, b) Cu. (c, d) Pt@Ni@Cu. (e, f) PtZn@Cu.

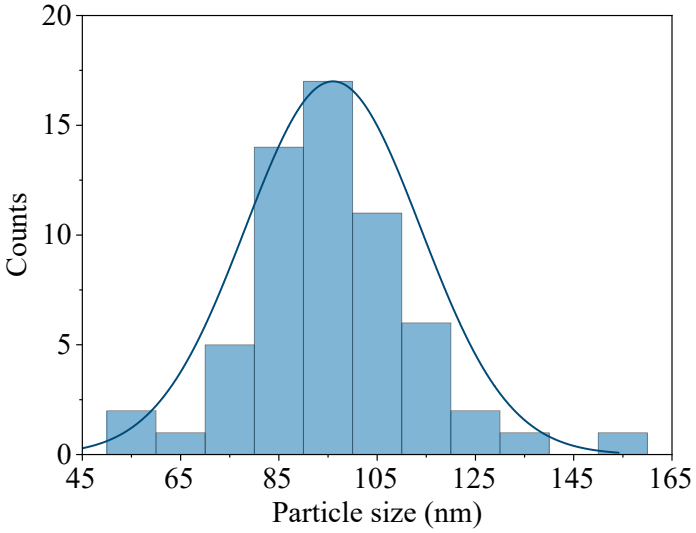

Fig. S9. Particle size distribution of PtNi@Cu.

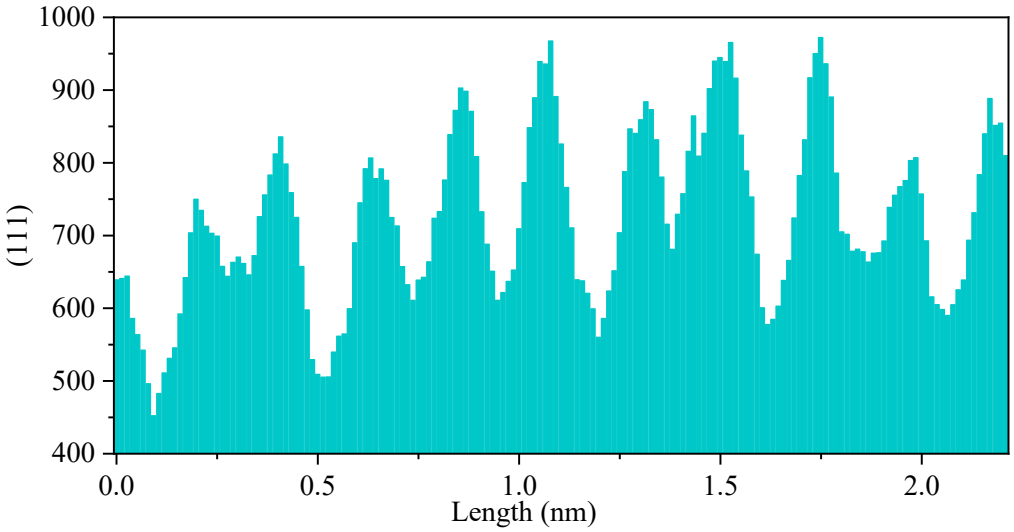

Fig. S10. Length of lattice fringe spacing on (111) surface.

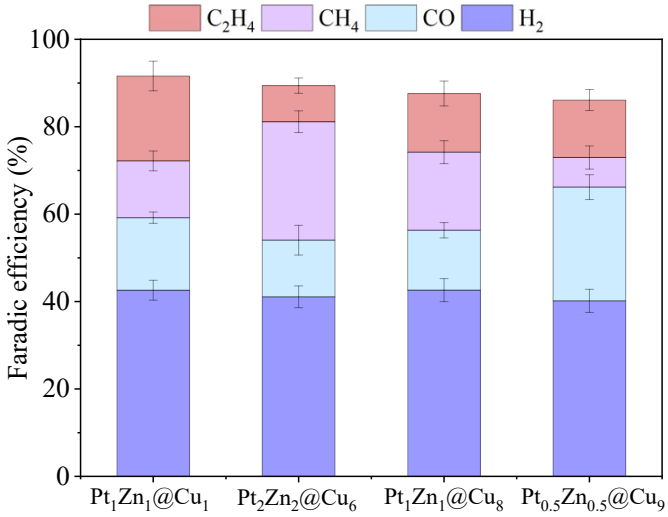

Fig. S11. Faradic efficiency of PtZn@Cu catalysts with different metal proportion.

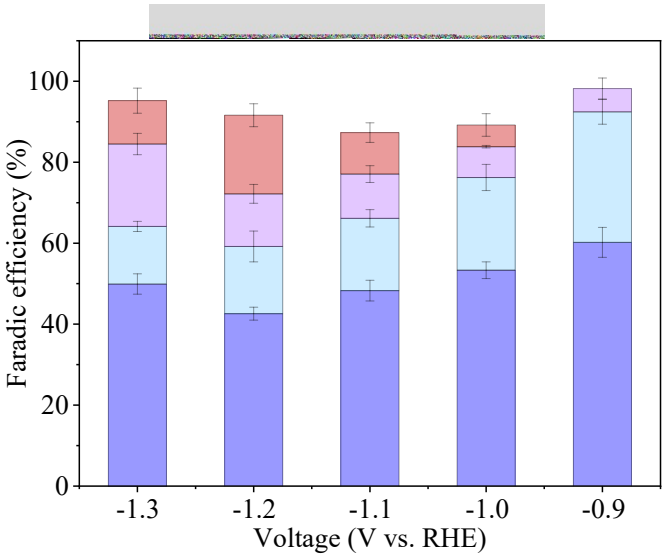

Fig. S12. Faradic efficiency of $Pt_1Zn_1@Cu_1$ at the potentials ranging from -0.9 V vs. RHE to -1.3 V vs. RHE.

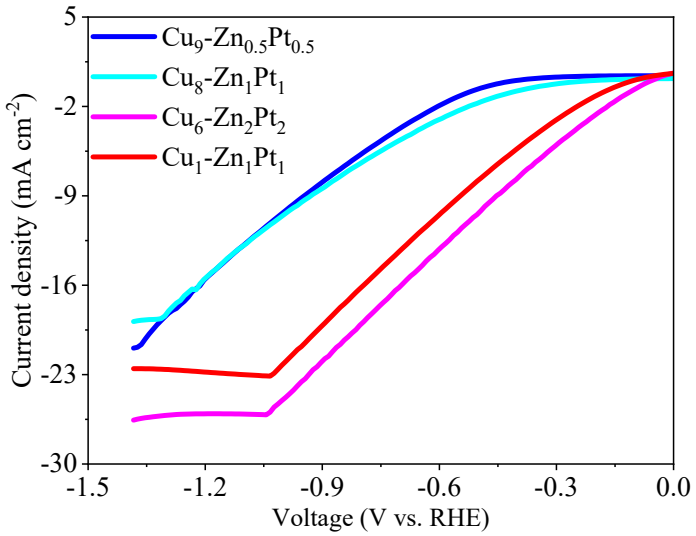

Fig. S13. Linear scan voltammetry curves of PtZn@Cu.

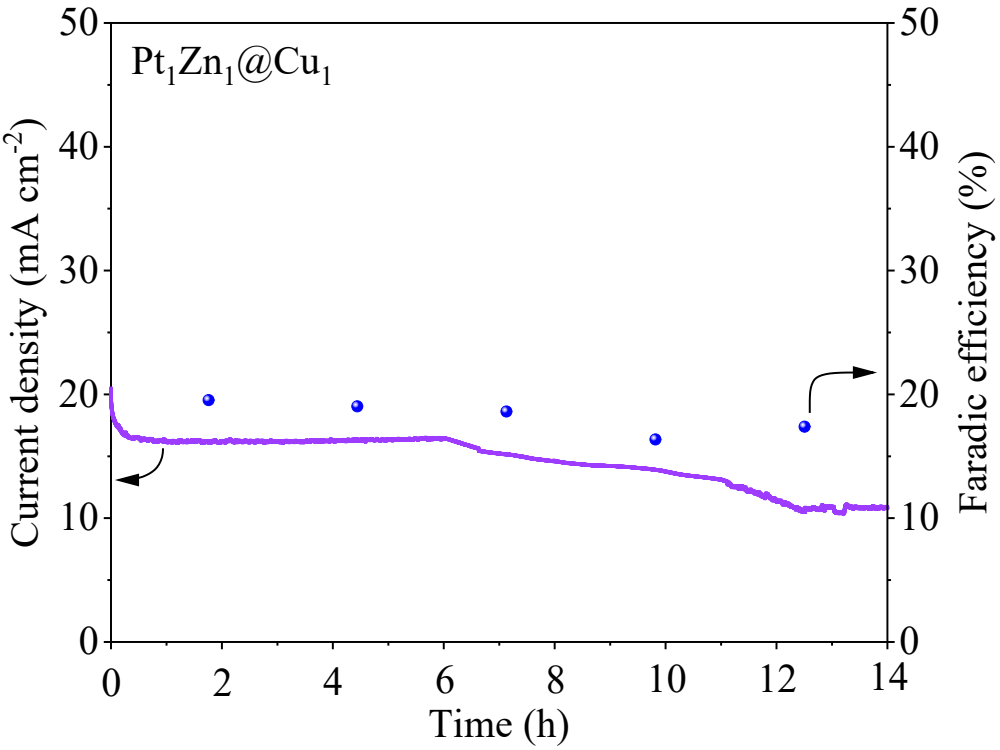

Fig. S14. Stability test of $Pt_1Zn_1@Cu_1$.

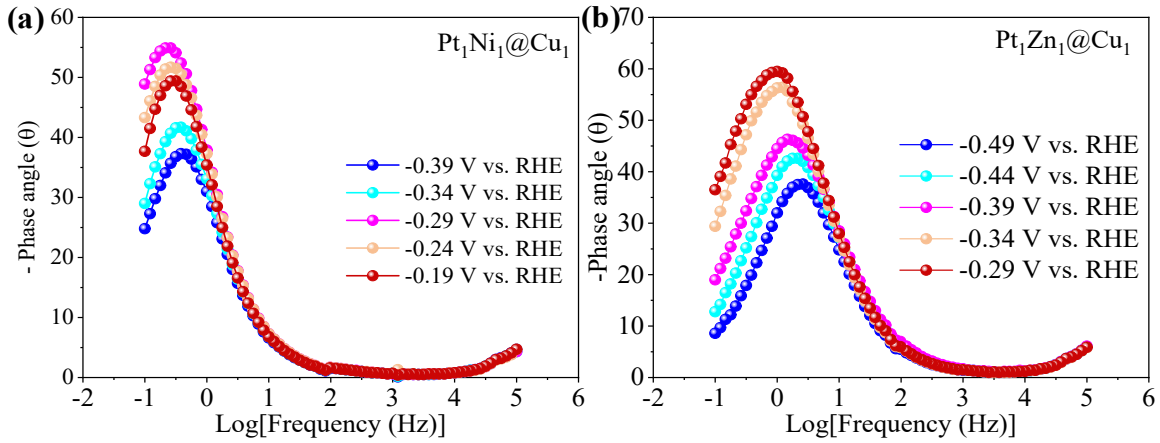

Fig. S15. Bode phase diagram of catalysts. (a) $Pt_1Ni_1@Cu_1$. (b) $Pt_1Zn_1@Cu_1$.

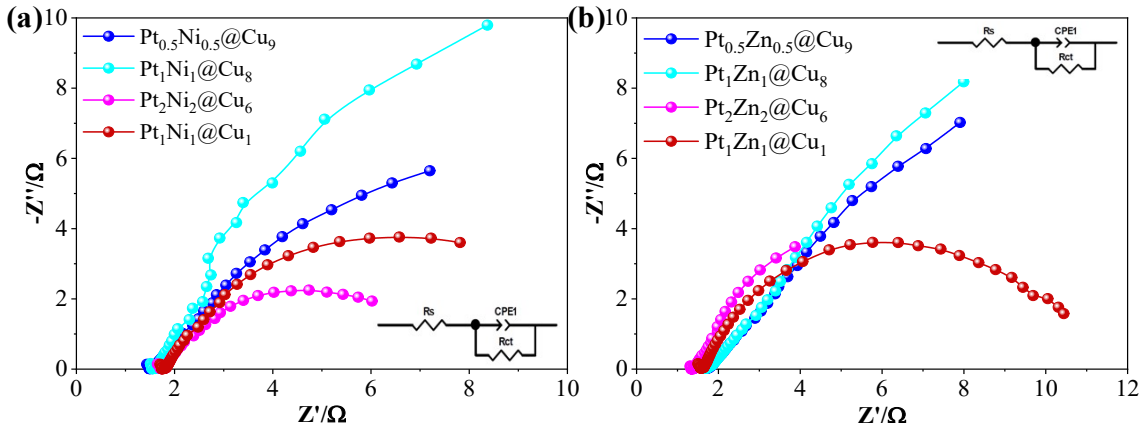

Fig. S16. Impedance spectrum of catalysts. (a) PtNi@Cu. (b) PtZn@Cu.

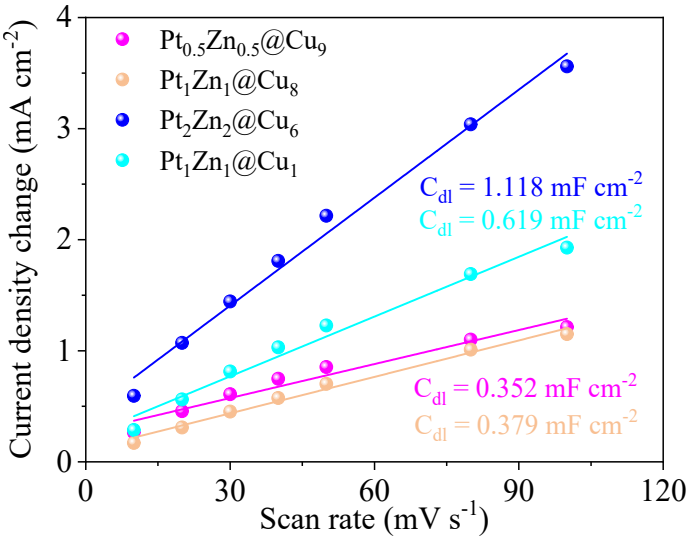

Fig. S17. Electrochemical surface area of PtZn@Cu catalysts.

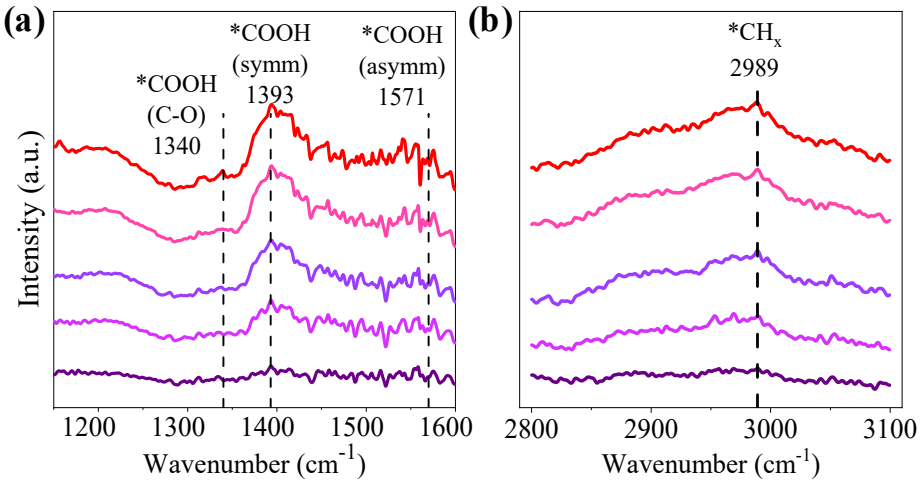

Fig. S18. *In-situ* FTIR spectra of PtNi@Cu catalyst.

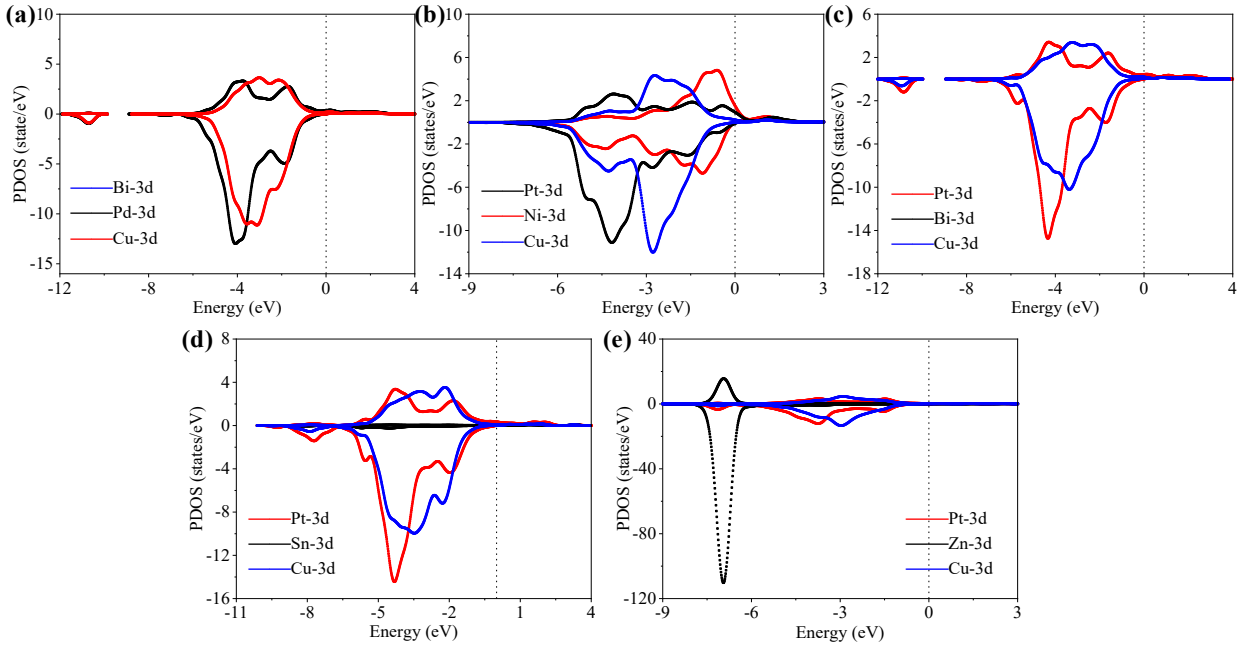

Fig. S19. Partial density of states of ternary alloy catalysts. (a) PdBi@Cu. (b) PtNi@Cu. (c) PtBi@Cu. (d) PtSn@Cu. (e) PtZn@Cu.

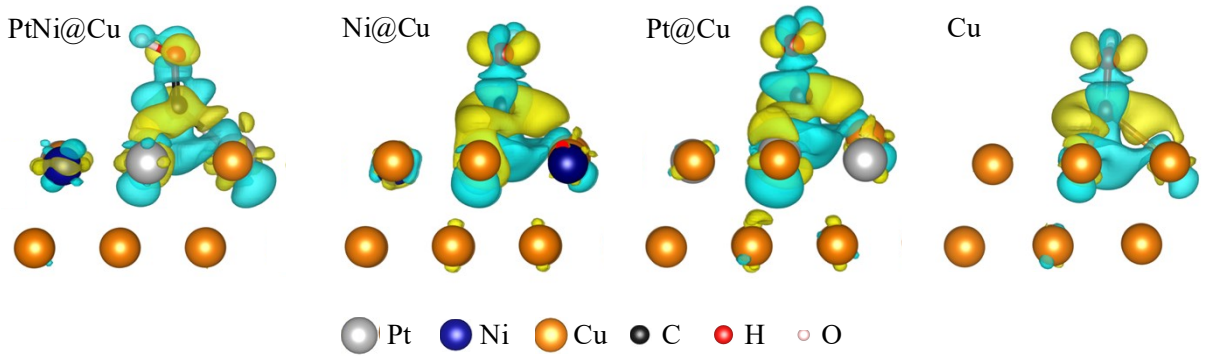

Fig. S20. The electron density difference plots of COH* adsorption on PtNi@Cu, Pt@Cu, Ni@Cu and Cu.

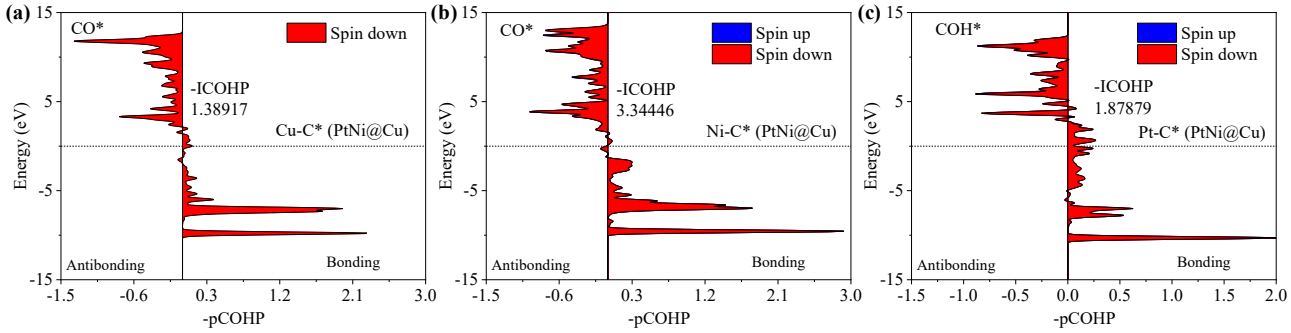

Fig. S21. COHP diagram of COH* adsorption on PtNi@Cu. (a) Cu-C COHP of COH* adsorption. (b) Ni-C COHP of COH* adsorption. (c) Pt-C COHP of COH* adsorption.

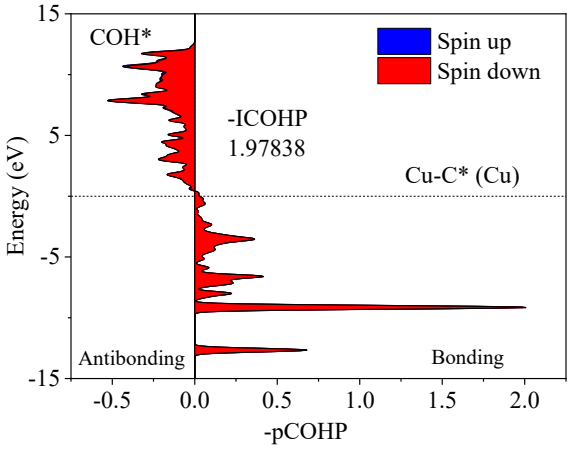

Fig. S22. COHP diagram of COH* adsorption on Cu.

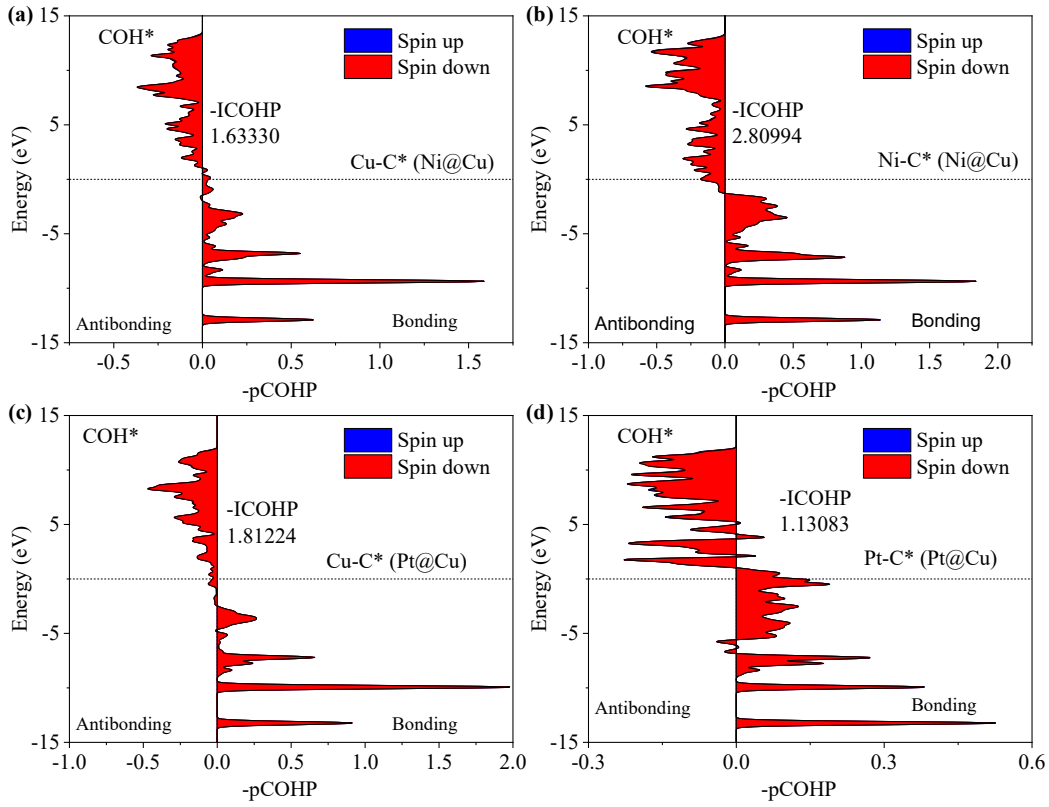

Fig. S23. COHP diagram of COH* adsorption on Ni@Cu and Pt@Cu. (a) Cu-C COHP of COH* adsorption on Ni@Cu. (b) Ni-C COHP of COH* adsorption on Ni@Cu. (c) Cu-C COHP of COH* adsorption on Pt@Cu. (d) Pt-C COHP of COH* adsorption on Pt@Cu.

Table S1. CO_2RR performance comparison of binary and ternary alloys.

Type	Catalysts	Products	FE (%)	J_i (mA cm^{-2})	Ref.
Binary alloy	Cu@Bi	HCOOH	91.27	-80.12	[1]
Binary alloy	IrSn	HCOO-	98	-78	[2]
Binary alloy	Cu-Ni	CO	98.8	-27.6	[3]
Binary alloy	Pd-Cu IM	C_1 products	64.95	~ -81	[4]
Binary alloy	CuZn	C_{2+} products	91	-136.5	[5]
Binary alloy	SnCu	C_{2+} products	79.3	-634.4	[6]
Ternary alloy	CuZnMn	CH_4	55	-418	[7]
Ternary alloy	AgCuAu	CO	~97	~ -145.5	[8]
Ternary alloy	AgCu	CO	~100	-3.9	[9]
Ternary alloy	CuAgNi	C_{2+} products	93.2	-818.1	[10]

Table S2. Percentage of element contents in PtNi@Cu and PtZn@Cu.

Catalysts	Cu 2p	Ni 2p	Zn 2p	Pt 4f
PtNi@Cu	31.38%	32.66%	-	35.96%
PtZn@Cu	33.88%	-	31.84%	34.29%

Table S3. The d-band center and M_1-M_2 bond length of different catalysts.

	BiPd@Cu	PtNi@Cu	PtSn@Cu	PtBi@Cu	PtZn@Cu
ε_d (M_1)	0	-2.77	-3.12	-2.97	-2.91
ε_d (M_2)	-2.87	-1.36	-1.92	0	-6.74
ε_d (Cu)	-2.78	-2.47	-2.84	-2.74	-2.70
d(M_1-M_2)	2.85	2.49	2.75	2.87	2.57

Reference

1 Zhang, Z.; Wang, L.; Yang, X.; Chu, M.; Huang, L.; Fan, J.; Xie, W.; Liu, D.; Yuan, W.; Situ, Y., *ACS Sustain. Chem. Eng.* **2024,** *12* (52), 18566-18576.

2 Yu, Q.; Wang, S.; Yang, X.; Li, X.; Chen, M.; Wang, W.; Li, X.; Huang, Y.; Zhang, T., *Mater. Today Energy* **2025,** *51*, 101901.

3 Cao, X.; Hu, Y.; Hui, D.; Zhang, K.; Chen, S.; Wei, L.; Ye, C.; Pan, G.; Hu, L., *ACS Appl. Nano Mater.* **2024,** *7* (14), 16264-16273.

4 Bagchi, D.; Riyaz, M.; Dutta, N.; Chawla, G.; R Churipard, S.; Kumar Singh, A.; C Peter, S., *Adv. Energy Mater.* **2024,** *14* (47), 2402237.

5 Zhang, J.; Guo, C.; Fang, S.; Zhao, X.; Li, L.; Jiang, H.; Liu, Z.; Fan, Z.; Xu, W.; Xiao, J.; Zhong, M., *Nat. Commun.* **2023,** *14* (1), 1298.

6 Liu, Y.; Yue, Z.; Jin, C.; Zheng, L.; Shi, J.; Li, D.; Wang, Y.; Bai, J.; Leng, K.; Wang, W.; Qu, Y.; Li, Q., *Small* **2025,** *21* (8), 2409259.

7 Chen, Y.; Lyu, N.; Zhang, J.; Yan, S.; Peng, C.; Yang, C.; Lv, X.; Hu, C.; Kuang, M.; Zheng, G., *Small* **2024,** *20* (15), 2308004.

8 Wang, Y.; Wang, B.; Ci, N.; Xie, R.; Chai, G.; Qiu, H.-J.; Zhang, Y., *ACS Appl. Nano Mater.* **2025,** *8* (12), 6085-6093.

9 Li, M.; Hu, Y.; Dong, G.; Wu, T.; Geng, D., *Small* **2023,** *19* (15), 2207242.

10 Jia, S.; Cheng, H.; Zhu, Q.; Chen, X.; Xue, C.; Deng, T.; Dong, M.; Xia, Z.; Jiao, J.; Chen, C.; Wu, H.; He, M.; Han, B., *Angew. Chem. Int. Ed.* **2025,** *64* (26), e202501833.